ELSEVIER

Journal of Photochemistry and Photobiology A: Chemistry 118 (1998) 111–122

Journal of Photochemistry and Photobiology A:Chemistry

The photo-oxidative degradation of sodium dodecyl sulphate in aerated aqueous TiO_2 suspension

Jimmy Lea, Adesoji A. Adesina*

Reactor Engineering and Technology Group, School of Chemical Engineering and Industrial Chemistry, University of New South Wales, Sydney, NSW 2052, Australia

Received 11 May 1998; received in revised form 31 July 1998; accepted 10 August 1998

Abstract

This paper reports the photocatalytic degradation of sodium dodecyl sulphate (SDS) in a bubble column reactor containing suspended irradiated ($\lambda = 250$–310 nm) titania particles. The effects of six major process variables were investigated. Reaction rate increased linearly with light intensity and the variation in temperature revealed an activation energy of about 41 kJ mol^{-1}. Although an increase in solution pH enhanced the hydrolysis of SDS and hence an increase in free dodecyl sulphate anion for adsorption, a downturn in rate was observed beyond pH = 7.5 probably due to reduced surface concentration of the dodecyl sulphate species on the predominantly negatively charged titania surface at pH values higher than the isoelectric point, IEP = 6. The optimum seen in the rate vs catalyst loading curve was also attributed to the compromise between increase in number of sites (particles) at higher catalyst concentration and the occurrence of light scattering and hence, reduced light-harvesting efficiency at these higher values. The data on the role of SDS concentration and oxygen partial pressure similarly suggest nonlinear dependency of rate on these reactants. The empirical models derived were consistent with the proposition of a dual-site (photogenerated positive and electron-rich sites) Langmuir–Hinshelwood mechanism where the rate-controlling step is the surface interaction between the adsorbed dodecyl sulphate and peroxy radicals. Highly reactive peroxy radicals were presumably formed from the protonation of surface superoxide anion, O_2^-, produced via adsorption of oxygen on the electron-rich site.

Keywords: Sodium dodecyl sulphate; Photodegradation; Titania; Bubble column reactor

1. Introduction

Many of the detergents used in the domestic and industrial laundry operations contain anionic-based surfactants such as alkyl aryl sulphonates and ester sulphates [1,2]. Anionics also find widespread use in the dairy and food industries as cleaning, disinfectant and antiseptic agents. Indeed, anionics constitute about 80% of the total surfactant production. With the western world alone producing an average annual output of more than 8 million tons of detergent, the accumulation of alkyl sulphate, notably, sodium dodecyl sulphate (SDS) as a primary pollutant in municipal waste water systems has attracted environmental concerns [3]. SDS is toxic to aquatic and animal life, hence it requires removal especially with increased emphasis on the concept of zero-pollutant discharge and the demand for high quality recycled water for both domestic and commercial applications. Although the presence of epilithic and planktonic bacteria in flowing rivers can facilitate the destruction of SDS [4], it is resistant to biodegradation in stationary water bodies and activated sludge due to microbial acclimatization [3]. Consequently, modern waste water treatment facilities must be supplemented with advanced oxidation technologies in order to meet stringent anti-pollution regulations.

The application of photocatalysis to the decontamination of wastewater containing highly toxic and recalcitrant organic compounds has burgeoned in the last decade [5–9]. Photocatalytic destruction has the advantages of low temperature operation (293–333 K), possibility for complete mineralization of even non-biodegradable species, relatively short reaction times, lowest reactor volume per unit throughput compared to other advanced oxidation processes (AOPs), opportunity for solar light utilization and relatively cheap catalyst (titania, haematite, zinc oxide) and non-hazardous oxidant, O_2. Recent reviews of the emerging role of photocatalysis in the development of novel waste processing and clean technologies are provided in [10,11]. To the best of our knowledge, the Hidaka group has carried out the most extensive investigation of the photodegradation of

*Corresponding author. Tel.: +61-2-9385-5268; fax: +61-2-9385-5966. e-mail: a.adesina@unsw.edu.au

1010-6030/98/$ – see front matter
PII: S1010-6030(98)00375-X

surfactant-bearing polluted aqueous systems [12–17]. Whilst the photocatalytic destruction of sodium dodecyl sulphate has not been previously examined, the recent study by Hidaka et al. [8,17] on dodecylbenzene sulphonate is instructive and signals the benefits of photocatalysis as an excellent accompaniment in water purification processes. Moreover, the commercial exploitation of novel wastewater treatment and recycling technologies is vital to Australia's economy since it is arguably the driest continent on the globe. These factors have furnished impetus for the present investigation.

Upon irradiation with light of appropriate energy (greater than or equal to the band gap of the semiconductor oxide), holes (positive vacancies, h^+_{vb}) and excited electrons, e^-_{cb}, migrate to the surface of the photocatalyst where they act as active centers by initiating or participating in redox reactions as electron donors or acceptors for species in solution. Obviously, light intensity will influence the population of these photogenerated entities and as a result, the ensuing redox reaction rates. However, unwanted hole and electron recombination may reduce the overall quantum efficiency of the photocatalytic process. Hori et al. [18] found that the quantum yield of CO production during selective photocatalytic reduction of CO_2 decreased almost exponentially with light intensity. On the other hand, Trillas et al. [19] observed that the percentage of 2,4-dichlorophenoxyacetic acid photodegraded over aqueous titania suspension was proportional to the square root of the radiation intensity suggesting a second order kinetics for the electron-hole recombination process. Okamoto and co-workers [20] reported the same behaviour for phenol oxidation. Even so, Wei and Wan [21] noted a departure from this parabolic relationship at higher intensities (>77% of the maximum) where the amount of phenol removed was linearly related to the light intensity. Interestingly, the photocatalytic degradation of crude oil in saline solution was unaffected by high irradiance (20–46 W m^{-2}) although the behaviour in the lower range (9–20 W m^{-2}) revealed a nonlinear increase in rate with illumination [22]. This mixed data suggest the ambiguities associated with the role of light intensity during photocatalysis.

Solute dissociation, catalyst surface charge and many physicochemical characteristics are affected by the presence of ions. Consequently, photocatalytic reactions in aqueous systems are strongly dependent on the pH of the medium. Dhananjeyan and collaborators [23] found that the photooxidation of thymine decreased with increasing pH. They ascribed this to a reduction in the oxidation potential of the h^-_{vb} site occasioned by a nernstian shift of the band edges to more negative values with increased alkalinity. The photoreduction of Cr(IV) was also favoured in strongly acidic solution (pH = 1) but at pH > 4, deactivation due to fouling by chromium hydroxides precipitated a rapid drop in reaction rate [24]. Nevertheless, the photodegradation of malonic acid improved with pH attaining a constant maximum at a value of 7 [25]. The photocatalytic oxidation of aqueous phenol over TiO_2 likewise gave maximum yields at pH = 8 [26] indicating that the pK value of the acid can shift the optimum medium pH even when the same photocatalyst is employed. Perhaps due to the nonionic nature of ethylbenzene, Vidal and colleagues [27] did not observe any effect of pH on the photocatalytic degradation of this organic compound.

In principle, increased catalyst loading would improve the concentration of active sites in slurry reactors and hence plot of the inverse catalyst loading against reciprocal of volumetric rate for various particle sizes may be used to delineate controlling resistances in the vessel [28]. However, light shielding and other secondary effects may confound this straightforward analysis in multiphase photoreactors. Indeed, slurry photoreactors are reportedly characterised by an optimum catalyst loading. Inel and Okte [25] obtained a maximum titania content of 0.8 g l^{-1} for malonic acid oxidation. They did not witness any significant change in CO_2 evolution beyond this value. The photocatalytic destruction of phenol also exhibited same dependency on catalyst loading [21].

Photocatalytic reaction mediated in liquid phase is a combination of solute dissociation, ion migration and adsorption–desorption surface reaction (ADS) steps [29]. Thus, the response to temperature changes is a 'hybrid' of the mildly linear influence corresponding to diffusion-controlled ion migration and the strongly exponential effect indicative of ADS steps. Additionally, in a multiphase photoreactor, the active sites are not thermally-activated and elementary steps often contain photogenerated species which are more labile and hence experience reduced energy barrier in the transformation to final products. Indeed, many workers have observed that photocatalytic reactions generally possess lower activation energy, E_A, values than similar conventional catalytic routes [30,31]. The data of Trillas et al. [19] on the photodegradation of 2,4-dichlorophenoxyacetic acid point to the possibility of a non-Arrhenius type dependency in photocatalytic systems.

As may be expected, photocatalytic kinetics is a function of the reactants, namely; organic substrate and the oxidant (or reductant). Dhananjeyan et al. [23] observed a first order rate dependency on thymine concentration. The photo-oxidation of phenol in several studies [7,21,26] also revealed an inhibitory effect of the organic on the rate of reaction. However, CO_2 production during the photomineralisation of malonic acid was linearly correlated with the acid concentration at lower values (<2 mM) but became independent of the substrate concentration at higher values [25].

Although direct oxygen attack of organic species in solution may lead to decomposition, dissolved O_2 also act as electron scavenger and hence mitigate in the hole/electron recombination rate to improve quantum yield of the photocatalytic reaction [29]. The photo-oxidative degradation of salicyclic acid has a maximum at about 60% O_2 [30] while an optimum composition of 20% O_2 was observed by Lu et al. [32] for the oxidation of dichlorovos.

As a result of these considerations, the effects of six major variables, viz., light intensity, pH, catalyst loading, temperature, SDS concentration and oxygen partial pressure, were examined in this paper in order to discern a plausible reaction mechanism and procure appropriate rate equation for the photo-oxidative process.

2. Experimental details

2.1. Materials and methods

Commercial titania powder (>99% anatase) supplied by Aldrich Chemicals was used as the photocatalyst. The physical properties of this catalyst have been given in a previous publication [33]. Sodium dodecyl sulphate (BDH Chemicals) and the NaOH and HCl used to adjust the pH of the initial slurry were all of analytical reagent grade. Solutions were prepared using Milli-Q triply distilled and deionised water. High purity O_2 and N_2 were obtained from BOC Gases, Sydney. Gas flow rates were controlled by Brooks electronic mass flowmeters. 2 ml samples were syringed at regular intervals from the reactor solution, microfiltered and chilled at 277 K overnight before analysis on a Waters Associate programmable ion chromatograph (model 590) equipped with a conductivity detector to measure free SO_4^{2-} concentration. An on-line TPS digital meter was used to monitor the pH change with time during reaction while light intensity was determined by a IL1400 radiometer/detector (International Light, Massachusetts) calibrated for 265–332 nm. Lamp spectral analysis provided by the vendor located a significant fraction of the radiation within the 250–310 nm window. In particular, since there was negligible emission beyond 500 nm, the possibility of direct absorption by SDS (at 655 nm) may be ruled out. About 1–2 drops of vegetable oil was always added to the reactor contents prior to each run to avoid foaming.

2.2. Reactor set-up

The annular photoreactor shown in Fig. 1 consisted of an outer cylindrical Pyrex casing (i.d. = 100 mm; height = 400 mm) fitted with a 20 μm hole gas distributor (glass). A UV mercury arc lamp suspended vertically by a tightly-fitted silicone rubber bung acting as a lid for the Pyrex casing is enclosed in a double-walled quartz U-tube through which chilled water flows (750 ml min^{-1}) to maintain reaction isothermality. The circulating water also ensured infrared filtering of the incident rays while nitrogen flushing of the lamp surface prevented accumulation of ozonised air in the reactor. The lamp may be operated at low (200 W), medium (300 W) and high (400 W) power levels. The slurry solution containing titania particles was placed between the annulus of the quartz U-tube and the Pyrex cylinder and O_2/N_2 mixture was bubbled through upwards through the porous glass distributor. Ports for pH and temperature measurements were provided as shown. Although the photoreactor was wrapped with aluminum foil, the entire assembly was further placed in a customized wooden chamber fitted with sliding plexiglass front door to minimize possible UV influence on the operator.

3. Results and discussion

3.1. Preliminary reactor considerations

The acquisition of reliable kinetic data from a multiphase reacting system may be readily supplanted by mass transport effects if the fluidodynamic characteristics are not properly selected. Additionally, for a slurry photoreactor, the light penetration depth is also a function of particle size and catalyst charge. In view of these complexities, preliminary runs were conducted to identify suitable range of conditions for the kinetic experiments. Separate blank runs performed under both aerobic and anaerobic conditions had revealed that measurable SDS degradation rates were only possible if UV, the TiO_2 photocatalyst and oxygen were all simultaneously present. Each run typically lasted 6 h in order to obtain time-invariant concentration measurements from the reactor contents. As may be seen in Fig. 2, more than 80% SDS conversion may be achieved within this period. This compares favourably with a biodegradation process which attained the same conversion in about 120 h [4]. The plot also shows a commensurate rise in free SO_4^{2-} ion concentration with SDS breakdown. It is evident that every mole of SDS degraded is matched by a corresponding release of SO_4^{2-} ion. This suggests that the anion was not being reused by intermediate compounds of the dodecyl oxidation such as alcohols. Since free SO_4^{2-} is more reliably measured than SDS concentration, reaction rate was therefore determined from the initial slope of the SO_4^{2-} concentration vs time curve. All experiments were carried out at a total pressure of 101 kPa.

Slurry reactors may exhibit gas–liquid, liquid–solid and intraparticle transport limitations. Based on experience from an earlier work [33], gas flow rate in excess of 400 ml min^{-1} was used to achieve efficient mixing and keep the photocatalyst particles (0.35 μm) in suspension. The transport criteria proposed in Ramachandran and Chaudhari [34] were employed for reactor diagnosis.

3.1.1. Gas–liquid (G–L) mass transfer resistance

In general, a bubble column reactor with porous plate distributor offers the best gas–liquid mass transfer coefficients [35], hence the use of a 20 μm sintered glass plate along with the relatively high gas flow rates (500 ml min^{-1}) recommended itself. The absence of gas–liquid transport limitation in a three-phase reactor may be assured if:

$$\frac{(-R_{SDS})}{k_L} a_L C^*_{O_2} < 0.1 \quad (1)$$

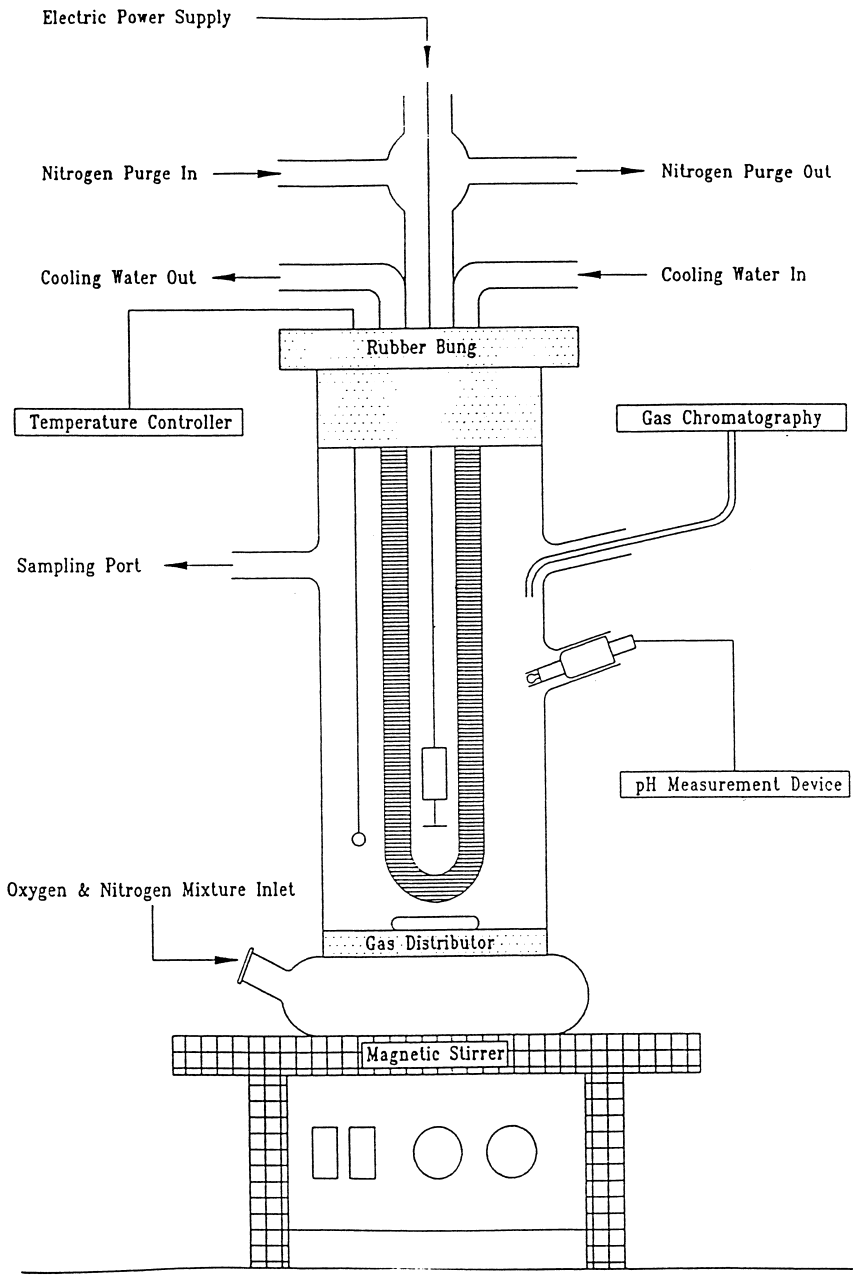

Fig. 1. The experimental photoreactor

Using parameter values given in Table 1 the LHS of Eq. (1) was evaluated as 0.069 and thus reactor operation indicated negligible G–L resistance. These fluidodynamic properties located the reactor operation in the homogeneous bubble flow regime. In fact, visual observation of the photoreactor confirmed the existence fine, well dispersed gas bubbles throughout the photoreactor.

3.1.2. Liquid–solid (L–S) mass transport effect

This type of transfer influence is minimal if

$$\frac{(-R_{SDS})}{k_s a_p C^*_{O_2}} < 0.1 \tag{2}$$

where a_P is defined,

$$a_p = \frac{6w}{\rho_p d_p} \tag{3}$$

Substitution of appropriate values from Table 1 gives the LHS as 2.43×10^{-5} which is much less than 0.1 as required. Interestingly, the Sherwood number, $k_s d_p/D_{eff}$, for this operation was essentially 2 – an indication that there was no shear stress between the particle and liquid. Thus, increased stirring speed (by the magnetic stirrer or gas agitation) would have no significant influence on the overall reaction rate. Clearly, the choice of gas flow rate and particle size was satisfactory.

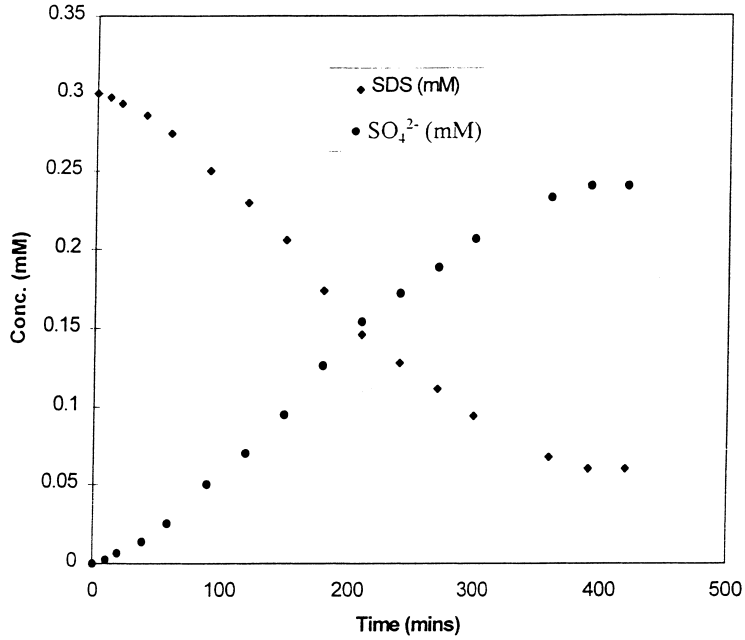

Fig. 2. Composition vs time curve for SDS and free SO_4^{2-} ion using 1 g cat l^{-1} with 80% O_2, pH = 7.5 at 293 K, I = 50 μE s^{-1}.

3.1.3. Intrapellet diffusion

Interference due to pore diffusional limitations may be ruled out if

$$\frac{d_p}{6}\left[\frac{(m+1)\rho_p(-R_{SDS})}{2D_{eff}wC^*_{O_2}}\right]^{1/2} < 0.2 \quad (4)$$

where for $m = 1$ and 2 the LHS yields 1.357×10^{-3} and 1.662×10^{-3}, respectively. Since most reactions hardly exceed second order ($m = 2$), it is evident that intrapellet transport resistance would be absent during kinetic investigation. Furthermore, the effectiveness factor, η, assuming first or second order kinetics, was estimated at approximately 1 irrespective of particle shape [28]. Sample calculations for the diagnostic analysis are shown in the Appendix A.

Table 1
Values of various parameters

Parameter	Value
$C^*_{O_2}$ (based on Henry's law, $p_A = Hx_A$)	3×10^{-7} mol cm^{-3} at $P_{O_2} = 0.3$ atm
H	4.75×10^4 atm for O_2 at 303 K
D_{AB}	2×10^{-5} cm^2 s^{-1}
D_{eff}	0.1 D_{AB}
d_T	10 cm
g	981 cm s^{-2}
ε_G	3.5×10^{-5}
$-R_{SDS}$	5×10^{-7} mol l^{-1} min^{-1} (at 30% O_2 and 0.5 g cat l^{-1}
ρ_G	1.2×10^{-3} g cm^{-3}
ρ_L	1.0 g cm^{-3}
ρ_p	3.9 g cm^{-3}
S_T	72 dyne cm^{-1}
S_{TW}	72 dyne cm^{-1}
μ_L	0.85 cP
μ_G	0.018 cP
u_G	0.106 cm s^{-1}
$u_{tp} = \frac{gd_p^2(\rho_p-\rho_L)}{18\mu_L}$	2.3×10^{-7} cm s^{-1}

3.2. Kinetic results

3.2.1. Effect of light intensity

Several investigators have reported the dependency of photocatalytic rates on light intensity [19–21,23]. Light intensity determines the degree of light absorption by the titania catalyst. Runs were carried out at the three light intensities corresponding to the three power levels for the lamp. At each setting, the intensity decreased exponentially with radial distance from the source. Thus, at any point within the annular reactor, the intensity, I, is given by

$$I = I_0 e^{-\beta r} \quad (5)$$

where I_0 is the maximum intensity for that particular power setting. For the commercial lamp used in this work, the data (not shown) were used to carry out the parametric estimation of β as 0.1005 cm^{-1} at all power levels. In a well-agitated slurry reactor, the average light intensity, I_{AV}, to which the catalyst particle is exposed may be easily derived as

$$I_{AV} = \frac{\int_{R_i}^{R_0} Ir\,dr}{\int_{R_i}^{R_0} r\,dr} \quad (6)$$

$$\frac{I_{AV}}{I_0} = \frac{2}{R_0^2}\left[\frac{1}{\beta^2} - \frac{e^{-\beta R_0}}{\beta}\left(\frac{1}{\beta} + R_0\right)\right] \quad (7)$$

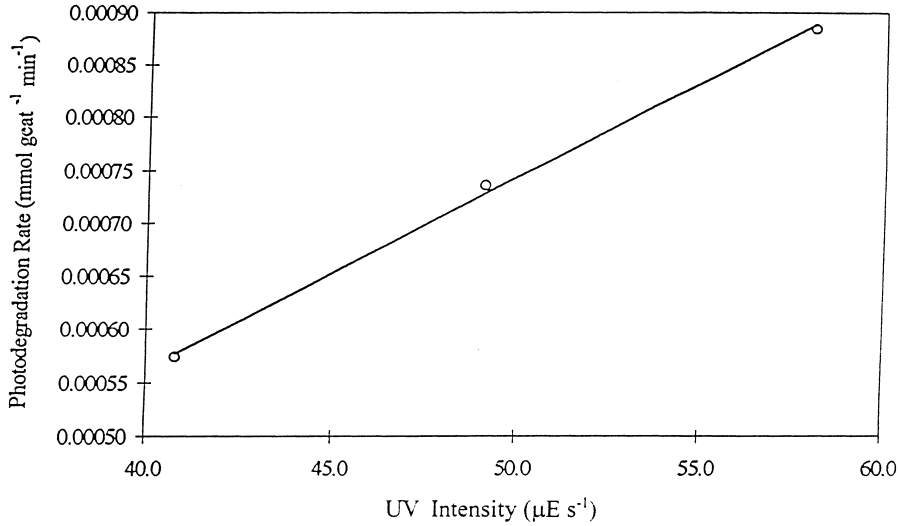

Fig. 3. Influence of light intensity with conditions: pH = 7.5, SDS conc = 0.3 mM, 1.0 g cat l^{-1}, 80% O_2 and $T = 293$ K.

which for $R_0 = 3$ cm (the annular width here) gave I_{AV}/I_0 as 0.82. This indicates adequate particle exposure to radiation within the reactor. Fig. 3 shows that the rate has a first order dependency on light intensity. Trillas et al. [26] had previously observed a linear relationship between extent of phenol elimination and light intensity. However, other workers [20,21] reported second order kinetics for the same reaction. The absorbed radiation in a reactor is a voluminal phenomenon and thus, the size of reactors used by individual laboratories may have affected the inferences. The role of light intensity is easily disguised in small photoreactors (<100 ml) [21]. Furthermore, for systems where the particle size for the porous catalyst is more than a few 100 nm, the radiation penetration depth is significantly reduced [36]. The present study has employed a relatively large photoreactor (1.25 l capacity) and a mean particle size of 350 nm which ensured that the local volumetric rate of energy absorption, LVREA, was constant from run to run. Light intensity was also measured by a digital radiometer rather than homogeneous actinometry which may yield misleading results [37].

3.2.2. Influence of slurry pH

The availability of holes and excited electrons on the surface of suspended TiO_2 particles promotes redox reactions with adsorbed electron donor or acceptor species. Thus, the pH of the initial slurry affects the rate of photodegradation of the organic substrate since the electric field associated with the solution pH alters the recombination rate of the hole/electron pair. Fig. 4 which plots the photodegradation rate as a function of the feed pH reveals that the SDS decomposition rate increased rapidly with slurry pH up to a maximum at about 7.5 and thereafter dropped rather gently. The rapid rise in rate with increased pH may be attributed to the higher hydrolysis rate of SDS with increasing alkalinity and hence the availability of free $C_{12}H_{25}OSO_3^-$ ions in solution for adsorption on the photocatalyst surface. However, this beneficial effect is compromised at pH values higher than the isoelectric point of titania in water (IEP = 6) where anion adsorption drops due to a predominantly negatively charged catalyst surface. We believe the optimum at pH = 7.5 was due to the interaction between these two opposing properties of the solid–liquid system.

3.2.3. Effect of catalyst loading

As earlier indicated, there was no measurable rate of reaction in the absence of titania. However, in a bubble column reactor with fixed upward gas flowrate, the limiting catalyst loading, W_{max}, to maintain solids suspension is given by

$$\frac{W_{max}}{\rho_L} = 6.8 \times 10^{-4} \frac{C_\mu d_T u_G \rho_G}{\mu_G} \left(\frac{S_T \varepsilon_G}{u_G \mu_L}\right)^{-0.23} \left(\frac{\varepsilon_G u_{tp}}{u_G}\right)^{-0.18} \gamma^3 \quad (8)$$

where,

$$C_{\mu=0.232-0.1788\ln\mu_L+0.1026(\ln\mu_L)^2} \quad (9)$$

and the gas hold-up, ε_G, is

$$\varepsilon_G = \frac{u_G (S_{TW}\rho_L/S_T)^{1/3}}{30 + 2u_G} \quad (10)$$

with γ having a value of nearly unity [34].

Employing the hydrodynamic and physicochemical properties listed in Table 1, W_{max} was estimated as 13 wt.% or 130 g of catalyst per litre for flow in the Stoke regime ($Re_p < 0.4$). It is manifest from Fig. 5 that the photodecomposition rate has both positive and negative orders with respect to the titania content. The increase in rate at low catalyst loading suggests that the addition of more titania particles improved the number of active sites in solution.

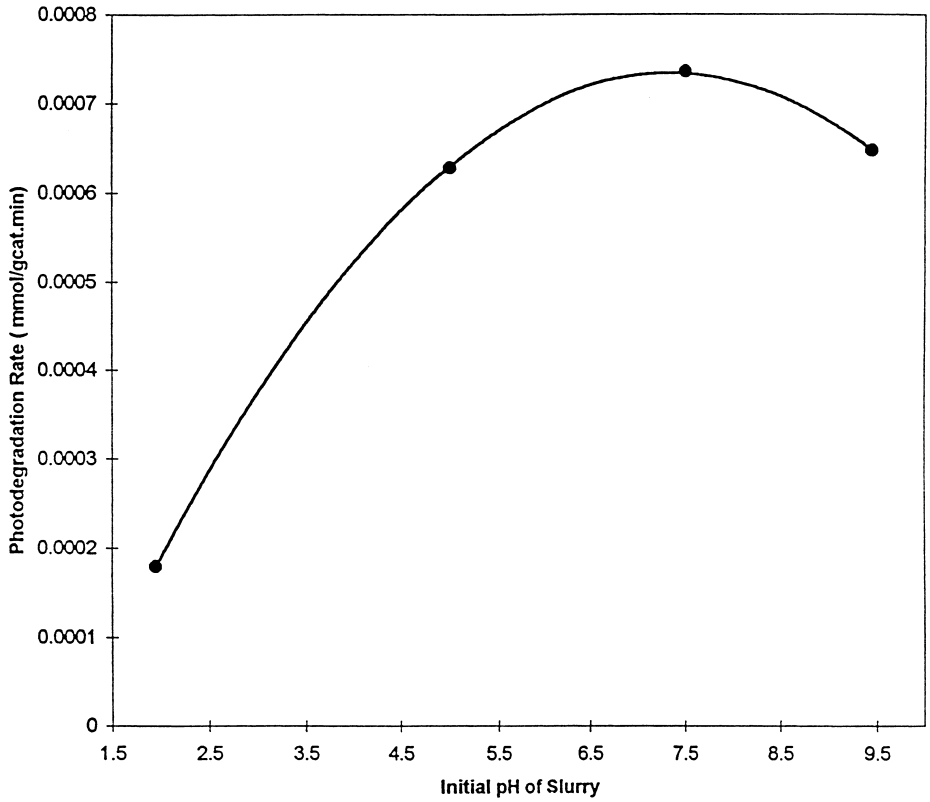

Fig. 4. Effect of slurry pH on photodegradation of SDS. Conditions: SDS conc = 0.3 mM, 1.0 g cat l^{-1}, 80% O_2 and T = 293 K, I = 50 μE s^{-1}.

Albeit, this positive change was confounded at loading levels higher than 1 g l^{-1} probably due to light scattering and shielding as the number of particles in solution increased. Furthermore, rate may drop as a result of loss in surface area available for light-harvesting occasioned by agglomeration (particle–particle interactions) at high solids concentration. These effects emphasize the additional complications involved in the design of large scale multi-phase photoreactors when compared to conventional slurry systems. For the present reactor, the data may be described by

$$-r_{SDS} = \frac{k_{cat}C_{cat}}{(\omega + C_{cat})^2} \tag{11}$$

where ω is a constant which was evaluated for this particular reactor as 1.0933 g cat l^{-1} while k_{cat} is a pseudo-rate con-

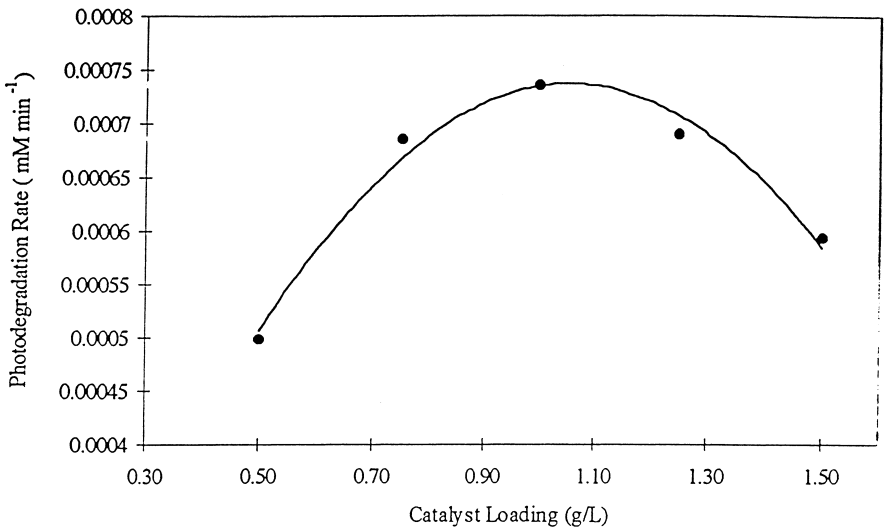

Fig. 5. Influence of catalyst loading on rate using SDS conc = 0.3 mM, pH = 7.5, 80% O_2 and T = 293 K, I = 50 μE s^{-1}.

stant measured as 9.073×10^{-6} mol g cat min^{-1} l^{-2} and a correlation coefficient of 0.987.

3.2.4. Influence of temperature

In general photocatalytic rates proceed at acceptable rates even at the relatively low temperatures of 293–333 K used in most studies. This is one of the major attractions of light-assisted catalytic reactions since new reaction pathways offering lower energy barriers may be stimulated. Fig. 6(a) shows the linear effect of temperature on the reaction over the range 293–313 K. Even so, an Arrhenius treatment of the data (cf. Fig. 6(b)) gave an activation energy, E_A, of 41.34 kJ mol^{-1} with a relatively high correlation coefficient of 0.9858. This low E_A value is consistent with the idea that the redox reactions involved in the photocatalytic route is supplemented by the non-thermal energy from photogenerated holes and electrons rather than heat-activated species or sites.

3.2.5. Effect of SDS concentration

The dependence of rate on SDS concentration was examined at pH = 7.5 using a feed gas containing 80% O_2/N_2 at 303 K with 1 g cat l^{-1} of titania. The behaviour shown in Fig. 7 suggests a nonlinear relationship between rate, $-r_{SDS}$, and the organosulphate concentration, C_{SDS}, which may be adequately expressed by

$$-r_{SDS} = \frac{K_{SDS} C_{SDS}}{(1 + K_{SDS} C_{SDS})^2} \tag{12}$$

with a maximum at about 0.5 mM. Regression analysis of

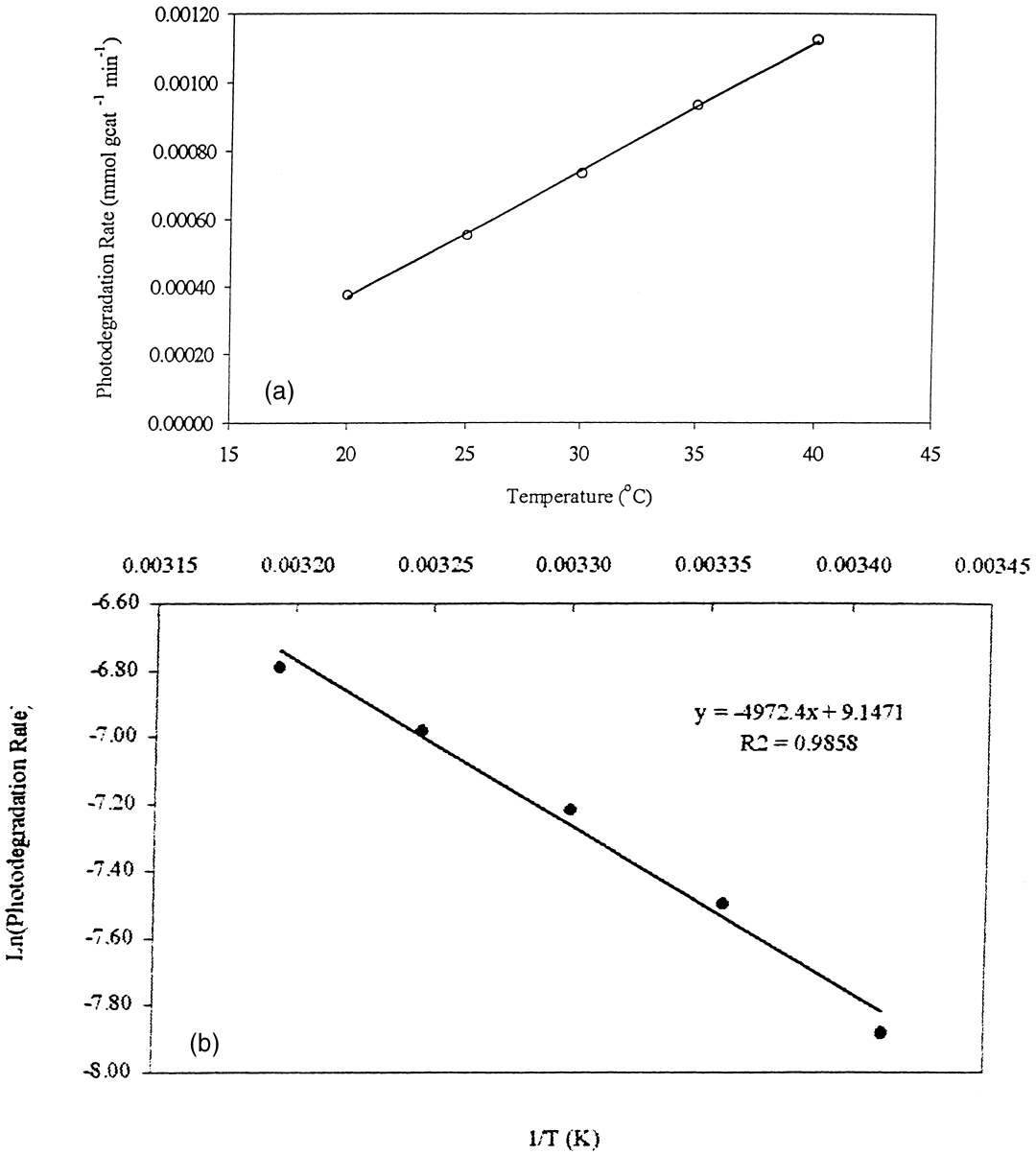

Fig. 6. Effect of temperature at SDS conc = 0.3 mM, pH = 7.5, 1.0 g cat l^{-1}, 80% O_2, I = 50 μE s^{-1} (b). Arrhenius plot.

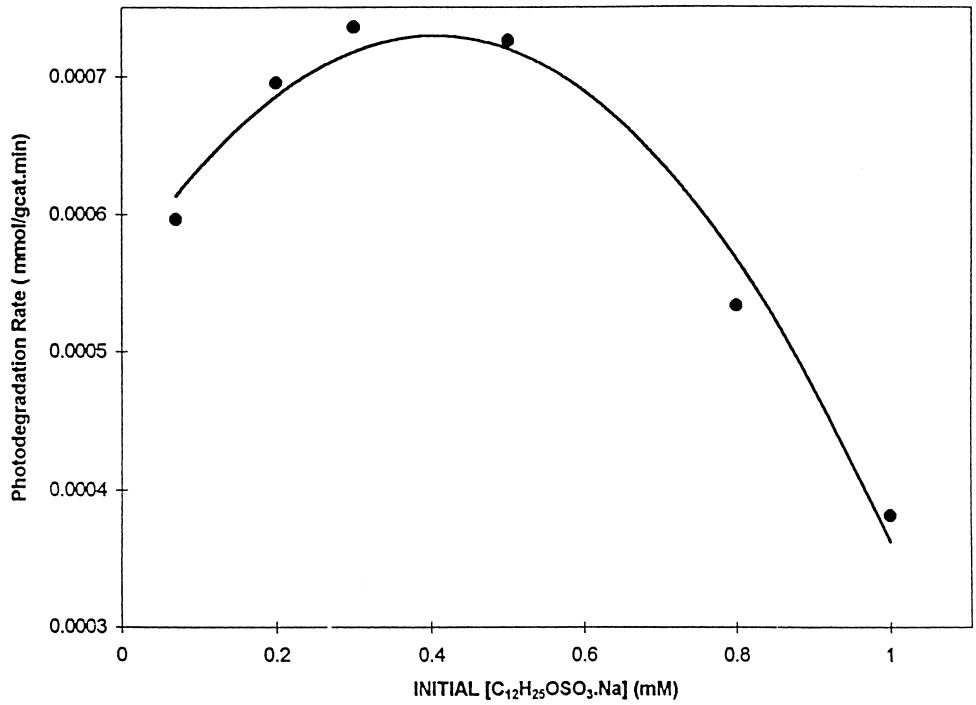

Fig. 7. Variation of photocatalytic degradation rate with initial SDS concentration using pH = 7.5, 1.0 g cat l^{-1}, 80% O_2 and T = 293 K, I = 50 μ s^{-1}.

the data gave the constants in Eq. (12) as; $k_{SDS} = 1.754 \times 10^{-2}$ l g cat min^{-1} and $K_{SDS} = 5.4885 \times 10^{-3}$ mol l^{-1} with a correlation coefficient of 0.994. It is apparent that the increase in rate at low SDS concentration is consistent with the high surface population of positive vacant sites for the organosulphate anion adsorption. Nevertheless, the inverse effect seen beyond 5×10^{-4} mol l^{-1} is symptomatic of inhibition due to the presence of oxidation intermediates such as carboxylic acids and alcohols arising from the dodecyl breakdown. Although the present analytical system could not monitor all individual intermediates (more than 20 possible different alcohols, acids, aldehydes and ketones), Sauer and Ollis [38] have indicated the photodecomposition of high molecular weight organics inevitably proceeds via these smaller and readily degradable units. Interestingly, the occurrence of a maximum photocatalytic rate at relatively high SDS concentration is evidence that the technology is applicable for wastewater treatment since typical industrial and municipal effluents do not have SDS levels above 40 ppm (0.133 mM).

3.2.6. Role of oxygen

These runs were performed using a slurry containing 0.3 mM of the SDS at pH = 7.5. As may be seen from Fig. 8 an increase in the O_2 partial pressure improved degradation rate but at a composition higher than 80% O_2, a deleterious effect was observed. Since the total gas flow rate ($O_2 + N_2$) was constant at 500 ml min^{-1} for all runs, this downturn in rate may not be ascribed to bubble coalescence at high O_2 flow rates as reported for phenol photocatalytic decomposition [21]. However, dissolved molecular oxygen is strongly electrophillic and thus increasing O_2 content probably reduced electron-hole recombination rate and hence the system was able to maintain favourable charge balance necessary for the photocatalytic-redox process. It is in fact evident from the reaction stoichiometry (Eqs. (13) and (14)) that a high O_2 : organosulphate molar ratio is required for complete mineralization to CO_2 and water.

$$C_{12}H_{25}OSO_3.Na + 18O_2 = 12CO_2 + 12H_2O + Na^+ + HSO_4^- \quad (13)$$

$$HSO_4^-(aq) + H_2O = SO_4^{2-}(aq) + H_3O^+(aq) \quad (14)$$

Nevertheless, in the presence of excess O_2, the semiconductor surface may become highly hydroxylated [29] to the point of inhibiting the adsorption of $C_{12}H_{25}OSO_3^-$ species. Moreover, the products of degradation such as SO_4^{2-}, HSO_4^-, $RCOO^-$, etc are all anions and would therefore reduce the effective liquid phase mobility and surface adsorption of oxygen. This may therefore be responsible for the drop in rate beyond 80% O_2/N_2. A fit of the data in Fig. 8 to the empirical model;

$$-r_{SDS} = \frac{K_{oxy}P_{oxy}}{(1 + K_{oxy}P_{oxy})^2} \quad (15)$$

yielded an excellent agreement with a correlation coefficient of 0.991 and parameter estimates, $k_{oxy} = 2.341 \times 10^{-8}$ mol min^{-1} g cat l^{-1} kPa^{-1} and $K_{oxy} = 1.0805 \times 10^{-2}$ kPa^{-1}.

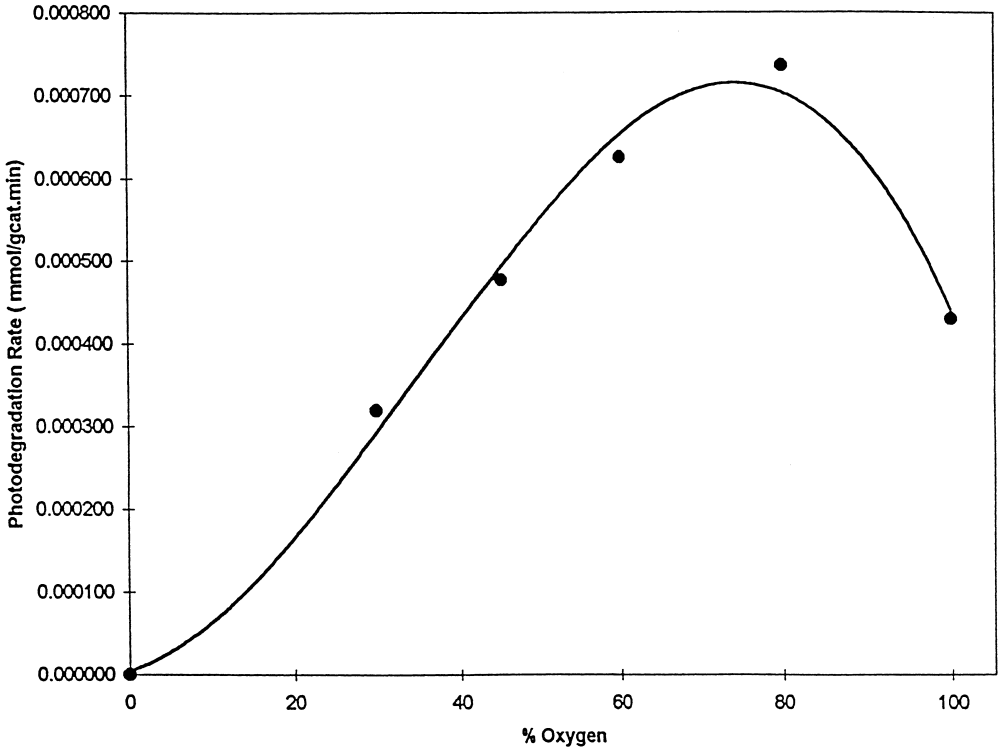

Fig. 8. Influence of oxygen partial pressure on rate. Conditions: SDS conc = 0.3 mM, pH = 7.5, 1.0 g cat l^{-1} and T = 293 K, I = 50 μE s^{-1}.

3.3. Proposed mechanism

From the preceding discussion, it is apparent that both photogenerated holes and electrons may migrate to the irradiated titania surface to act as adsorption sites or receptors for the dodecyl sulphate ion and molecular oxygen. Hydroxy or peroxy surface radicals formed from the protonation of the superoxide O_2^- anion (arising from adsorption of molecular oxygen on electron-rich sites) are highly reactive and may readily attack the chemisorbed organosulphate ion to release aqueous HSO_4^- and a surface carboxylate radical which undergoes successive decarboxylation and hyroxylation to alcohols, aldehydes and CO_2 [38]. Due to steric effects, we assume that the primary degradation of the bulky dodecyl sulphate to surface carboxylate and hydrogen sulphate radicals is the rate-controlling step, rcs, (cf. Eq. (23)) in the following sequence of elementary reactions.

$$TiO_2 + hv = h^+_{vb} + e^-_{cb} \quad (16)$$

$$C_{12}H_{25}OSO_3.Na(aq) = C_{12}H_{25}OSO_3^-(aq) + Na^+(aq) \quad (17)$$

$$O_2 + e^-_{cb} = O_2^-(ads) \quad (18)$$

$$H_2O + h^+_{vb} = OH^\bullet(ads) + H^+(aq) \quad (19)$$

$$O_2^-(ads) + H^+(aq) = HO_2^\bullet(ads) \quad (20)$$

$$HO_2^\bullet(ads) + H^+(aq) = 2OH^\bullet(aq) + h^+_{vb} \quad (21)$$

$$C_{12}H_{25}OSO_3^-(aq) + h^+_{vb} = R_nOSO_3^\bullet(ads) \quad (22)$$

$$R_nOSO_3^\bullet(ads) + HO_2^\bullet(ads) = R_{n-1}COO^\bullet(ads) + OHSO_3^\bullet(ads) \quad (23)$$

$$OHSO_3^\bullet(ads) = HSO_4^-(aq) + h^+_{vb} \quad (24)$$

$$HSO_4^-(aq) + H_2O = SO_4^{2-} + H_3O^+(aq) \quad (25)$$

$$R_{n-1}COO^\bullet(ads) = R^\bullet_{n-1}(ads) + CO_2 \uparrow \quad (26)$$

$$R^\bullet_{n-1}(ads) + O_2^-(ads) = R_{n-2}COO^\bullet(ads) + e^-_{cb} \quad (27)$$

$$R^\bullet_{n-1}(ads) + OH^\bullet(aq) = R_{n-1}OH(aq) + TiO_2 \quad (28)$$

$$HCOO^\bullet(ads) + OH^*(aq) = H_2O + CO_2 + TiO_2 \quad (29)$$

$$h^+_{vb} + e^-_{cb} = TiO_2 + \text{heat} \quad (30)$$

Assuming that the organosulphate ion and the protonated superoxide anion ($OH^\bullet$ or $HO_2^\bullet$), are the most abundant reactive intermediates (MARI), and all other steps except the rcs are either in quasi-equilibrium or rapid, one can readily derive an appropriate rate expression for the dual-site (hole- and electron-rich) Langmuir–Hinshelwood mechanism as [39];

$$-r_{SDS} = \frac{k_{rxn}C_{SDS}P_{oxy}}{\left[(1 + K_{SDS}C_{SDS})(1 + K_{oxy}P_{oxy})\right]^2} \quad (31)$$

Incidentally, an identical rate law may be obtained from the experimental data by combining Eqs. (12) and (15). Since the present runs were performed by varying one factor while all others were kept constant, it is statistically inept to obtain an independent validation of Eq. (31) from a combined data set. Even so, correlation coefficient of $\geq$0.99 determined for

a fit of the data to individual Eqs. (12) and (15) provides reasonable justification for the mechanistic proposal.

4. Conclusions

We have demonstrated that the photocatalytic degradation of sodium dodecyl sulphate can be carried out in aqueous titania suspension at ambient conditions with maximum rates at neutral pH. The relatively high demand for oxygen (80% O_2/N_2) is consistent with a stoichiometrically high oxygen : organosulphate ratio for complete mineralisation. Photodegradation rate exhibited strong nonlinearity with respect to catalyst loading and SDS concentration although there seemed to be a first order dependency on light intensity. The reaction was also characterised by a relatively low activation energy of about 41 kJ mol^{-1}. It is proposed that the photodegradation proceeds via a dual-site mechanism involving the adsorption of O_2 and the dodecyl sulphate anion on electron-rich and positive vacant sites, respectively. Surface reaction between adsorbed peroxy or hyrdoxy radicals and the adsorbed organosulphate to give carboxylate group appeared to be the rate-controlling step. Further successive attack of the surface carboxylate by these highly reactive radicals can lead to the formation of alcohols, aldehydes and the final oxidation products of CO_2, H_2O and SO_4^{2-}.

5. Nomenclature

a_L	gas–liquid interfacial area per unit volume of reactor (cm^{-1})
a_p	solid catalyst area per unit volume of reactor (cm^{-1})
$C^*_{O_2}$	bulk liquid phase O_2 concentration in equilibrium with the gas phase O_2 (mol cm^{-3})
d_p	catalyst particle diameter (cm)
d_T	reactor diameter (cm)
D_{AB}	diffusivity of oxygen in water at 303 K ($cm^2\ s^{-1}$)
D_{eff}	effective diffusivity inside the particle ($cm^2\ s^{-1}$)
E_A	activation energy (kJ mol^{-1})
g	acceleration due to gravity (cm s^{-2})
I	light intensity (μE $m^{-2}\ s^{-1}$)
I_0	maximum light intensity (μE $m^{-2}\ s^{-1}$)
k_L	liquid film mass transfer coefficient (cm s^{-1})
k_{cat}	pseudo rate constant with respect to the catalyst
k_{oxy}	pseudo rate constant with respect to oxygen
k_{SDS}	pseudo rate constant with respect to the dodecyl sulphate
k_s	liquid-to-catalyst mass transfer coefficient (cm s^{-1})
K_{SDS}	adsorption equilibrium constant for dodecyl sulphate ions
K_{oxy}	adsorption equilibrium constant for oxygen
P_{oxy}	oxygen partial pressure (kPa)
$-r_{SDS}$	photodegradation rate of sodium dodecyl sulphate (m mol g $cat^{-1}\ min^{-1}$)
$-R_{SDS}$	photodegradation rate of SDS (mmol $l^{-1}\ min^{-1}$)
S_T	liquid surface tension (dyne cm^{-1})
S_{TW}	water surface tension (dyne cm^{-1})
u_G	superficial gas velocity to reactor (cm s^{-1})
u_{tp}	particle terminal velocity in reactor (cm s^{-1})
W_{max}	maximum catalyst loading suspended in a bubble column reactor (g l^{-1})

Greek symbols

β	parameter in Eq. (5)
ε_G	gas hold-up
γ	wettability factor (essentially 1 for most catalysts)
η	effectiveness factor
μ_G	gas viscosity (g $cm^{-1}\ s^{-1}$)
μ_L	liquid viscosity (g $cm^{-1}\ s^{-1}$)
ρ_L	liquid density (g cm^{-3})
ρ_p	particle density (g cm^{-3})
ω	parameter in Eq. (11)

Acknowledgements

The authors appreciate the technical assistance given by Kate Nasev and Andrew Chau. We are also grateful to the Australian Research Council for financial support of this project.

Appendix A

Computation of k_La_L from Akita and Yoshida's correlation [34]

$$k_L a_L = 0.6 D_{AB}^{0.5} \left(\frac{\mu_L}{\rho_L}\right)^{-0.12} \left(\frac{S_T}{\rho_L}\right)^{-0.62} d_T^{0.17} g^{0.93} \varepsilon_G^{1.1} \qquad \text{(A.1)}$$

which yields, upon substitution of values from Table 1, $k_L a_L = 5.97 \times 10^{-4}$ cm s^{-1}.

Estimation of Sherwood number, Sh

The Sherwood number is given by the Kobayashi–Saito correlation [34] as;

$$\mathrm{Sh} = \frac{k_s d_p}{D_{AB}} = 2 + 0.212 \left[\frac{d_p^3(\rho_p - \rho_L)g}{\mu_L D_{AB}}\right]^{1/3} \left[\frac{d_p u_G \rho_L}{\mu_L}\right]^{0.112} \qquad \text{(A.2)}$$

from whence Sh = 2.0018 after appropriate substitution. Thus, $k_S = 2D_{AB}/d_p = 1.143$ cm s^{-1}

References

[1] D.A. Karsa (Ed.), The Industrial Applications of Surfactants: Special Publication 59, Royal Society of Chemistry, London, 1987.

[2] W.M. Lindfield (Ed.), Anionic Surfactants, Surfactant Sci. Ser. 7 (1976) 135.
[3] J.I. Kroschwitz, M. Howe-Grant (Eds.), Kirk-Othmer Encylopedia of Chemical Technology, 4th ed., vol. 7–8, Wiley, 1994.
[4] D.J. Anderson, M.J. Day, N.J. Russell, G.F. White, Appl. Environ. Microbiol. 56(3) (1990) 758.
[5] E. Pelizzetti, N. Serpone (Eds.), Photocatalysis: Fundamentals and Applications, Wiley, New York, 1991.
[6] R. Matthews, S.R. McEvoy, J. Photochem. Photobiol. A Chem. 66 (1992) 355.
[7] R. Matthews, S.R. McEvoy, J. Photochem. Photobiol. A Chem. 64 (1992) 231.
[8] H. Hidaka, J. Zhao, S. Horikoshi, N. Serpone, E. Pelizzetti, Yukagaku 44(2) (1995) 121.
[9] D.F. Ollis, E. Pelizzetti, N. Serpone, Environ. Sci. Tech. 25 (1991) 1523.
[10] V.N. Parmon (Ed.), Photocatalysis and Solar Energy Conversion, Catal. Today 39(3) (1997) 137.
[11] R.F. Howe, Dev. Chem. Eng. Min. Proc: The Aust. Res. J. 6 (1998) 55.
[12] H. Hidaka, J. Zhao, Y. Satoh, K. Nohara, E. Pelizzetti, N. Serpone, J. Mol. Catal. 88(2) (1994) 239.
[13] H. Hidaka, J. Zhao, Y. Satoh, K. Nohara, E. Pelizzetti, N. Serpone, J. Photochem. 35 (1986) 219.
[14] H. Hidaka, J. Zhao, Y. Satoh, K. Nohara, E. Pelizzetti, N. Serpone, J. Photochem. Photobiol. A Chem. 42 (1988) 375.
[15] H. Hidaka, K. Nohara, J. Zhao, K. Takashima, E. Pelizzetti, N. Serpone, New J. Chem. 18(4) (1994) 541.
[16] H. Hidaka, K. Nohara, J. Zhao, K. Takashima, E. Pelizzetti, N. Serpone, Nouv. J. Chem. 9 (1985) 67.
[17] H. Hidaka, J. Zhao, K. Nohara, K. Kitamura, Y. Satoh, E. Pelizzetti, N. Serpone, in: D.F. Ollis, H. Al-Ekabi (Eds.), Photocatalytic Purification and Treatment of Water and Air, Elsevier, New York, 1994, p. 251.
[18] H. Hori, F.P.A. Johnson, K. Koike, O. Ishitani, T. Ibusuki, J. Photochem. Photobiol. A Chem. 96 (1996) 171.
[19] M. Trillas, J. Peral, X. Domenech, Appl. Catal. B Environ. 5 (1995) 377.
[20] K.I. Okamoto, Y. Yamoto, H. Tanaka, M. Tanaka, Bull. Chem. Soc. Japan 58 (1985) 2015.
[21] T.-Y. Wei, C.-C. Wan, Ind. Eng. Chem. Res. 30 (1991) 1293.
[22] M. Nair, Z. Luo, A. Heller, Ind. Eng. Chem. Res. 32 (1993) 2318.
[23] M.R. Dhananjeyan, R. Annapoorani, S. Lakshmi, R. Renganathan, J. Photochem. Photobiol. A Chem. 96 (1996) 187.
[24] J. Gimenez, M.A. Aguado, S. Cervera-March, J. Mol. Catal. A Chem. 105 (1996) 67.
[25] Y. Inel, A.N. Okte, J. Photochem. Photobiol. A Chem. 96 (1996) 175.
[26] M. Trillas, M. Pujol, X. Domenech, J. Chem. Tech. Biotech. 55 (1992) 85.
[27] A. Vidal, J. Herrero, M. Romero, B. Sanchez, M. Sanchez, J. Photochem. Photobiol. A Chem. 79 (1994) 213.
[28] H.S. Fogler, Elements of Chemical Reaction Engineering, 2nd ed., Prentice-Hall, Englewood Cliffs, NJ, 1992.
[29] R.L. Pozzo, M.A. Baltanas, A.E. Cassano, Catal. Today 39 (1997) 219.
[30] A. Mills, C.E. Holland, R.H. Davies, D. Worsley, J. Photochem. Photobiol. A Chem. 83 (1994) 257.
[31] G.R. Bamwenda, S. Tsubota, T. Kobayashi, M. Haruta, J. Photochem. Photobiol. A Chem. 77 (1994) 59.
[32] M.-C. Lu, G.-D. Roam, J.-N. Chen, C.P. Huang, J. Photochem. Photobiol. A Chem. 76 (1993) 103.
[33] H. Wang, A.A. Adesina, Appl. Catal. B Environ. 14 (1997) 241.
[34] P.A. Ramachandran, R.V. Chaudhari, Three-Phase Catalytic Reactors, Gordon and Breach, New York, 1983.
[35] W.D. Deckwer, Y. Louisi, A. Zaidi, M. Ralek, Ind. Eng. Chem. Proc. Des. Dev. 19 (1980) 699.
[36] C.A. Martin, M.A. Baltanas, A.E. Cassano, J. Photochem. Photobiol. A Chem. 76 (1993) 199.
[37] M.I. Cabrera, O.M. Alfano, A.E. Cassano, Ind. Eng. Chem. Res. 33 (1994) 3031.
[38] M. Sauer, D.F. Ollis, J. Catal. 149 (1994) 81.
[39] M. Boudart, M. Djega-Maridassou, Kinetics of Heterogeneous Catalytic Reactions, Princeton University Press, Princeton, NJ, 1984.